Crystal Structures and Melting Behaviors of 2D and 3D Anionic Coordination Polymers Containing Organometallic Ionic Liquid Components

Kimata, Hironori

Mochida, Tomoyuki

(Citation)
Chemistry-A European Journal,25(43):10111-10117

(Issue Date)
2019-08-01

(Resource Type)
journal article

(Version)
Accepted Manuscript

Crystal Structures and Melting Behaviors of 2–D and 3–D Anionic Coordination Polymers Containing Organometallic Ionic Liquid Components

Hironori Kimata, and Tomoyuki Mochida*[a]

[a]*Department of Chemistry, Kobe University, Rokkodai, Nada, Kobe, Hyogo 657-8501 (Japan). E-mail: tmochida@platinum.kobe-u.ac.jp*

Abstract: Although coordination polymers generally do not melt, several that do melt have been synthesized recently and have drawn much attention. In this study, we synthesized two- and three-dimensional coordination polymers that melt, $[Ru(Cp)(C_6H_5R)][M\{C(CN)_3\}_2]$ (R = H, Me, Et; M = K, Rb; Cp = C_5H_5), which are complex salts comprising $M[C(CN)_3]$ and organometallic ionic liquids $[Ru(Cp)(C_6H_5R)][C(CN)_3]$. They have anionic $[M\{C(CN)_3\}_2]^-_n$ coordination polymer frameworks, whose dimensionalities depend on the size of the organometallic cation inside. Their melting points decreased with increasing cation substituent length and size of the alkali metal ion (T_m = 102–239 °C), and these low-melting-point coordination polymers exhibited incongruent melting, forming mixtures of solid $M[C(CN)_3]$ and ionic liquid upon melting. Using the same method, we also synthesized coordination polymers with various bridging ligands, $[Co(Cp)_2][MX_2]$ (X = $B(CN)_4$, $C(CN)_3$, $N(CN)_2$; M = K, Na), and a paramagnetic coordination polymer, $[Fe(Cp)_2][K\{C(CN)_3\}_2]$.

Introduction

In recent decades, research on coordination polymers or metal organic frameworks has been conducted extensively, particularly in view of the development of applications based on their porosity.[1] Although coordination polymers generally do not melt, some that do melt have been developed recently and have attracted much attention.[2] They are intriguing materials owing to glass-forming properties, phase transformations, and processability, which enable the modification of ion transport and structural properties through doping, hybridization, and defect control.[3-5] There are approximately a dozen 1–D coordination polymers that melt, some of which even exhibit melting points below 100 °C.[3] However, only a few 2–D and 3–D coordination polymers that can melt have been reported, [4,5] such as $[Zn(H_2PO_4)_2(triazole)_2]$ (T_m = 180 °C)[4a] and $[Zn(Im)_4]$ (T_m = 592 °C)[5a], which display higher melting points. Therefore, it is important to explore a method to construct 2–D or 3–D coordination polymers with low melting points, the development of which would lead to various applications characteristic of soft crystals.[6]

In this study, we developed 2–D and 3–D coordination polymers that melt by incorporating organometallic ionic liquid components. Ionic liquids are salts with melting points below 100 °C.[7] Although most of them are onium salts, we have developed various organometallic ionic liquids that contain cationic sandwich complexes.[8] The organometallic cations and polycyano anions used in this study are shown in Figure 1. Importantly, the polycyano anions can act as both counter anions for the ionic liquids[9] and bridging ligands for the coordination polymers.[10] This paper describes the preparation, structures, and melting behaviors of coordination polymers $[Ru(Cp)(C_6H_5R)][M\{C(CN)_3\}_2]$ (R = H, Me, Et; M = K, Rb; Cp = C_5H_5), shown in Figure 2a, which are complex salts comprising $M[C(CN)_3]$ and ionic liquids $[Ru(Cp)(C_6H_5R)][C(CN)_3]$. They have anionic coordination polymer frameworks and accommodate organometallic cations. It has been well known that anionic coordination polymers exhibit intriguing structural diversity and functionalities.[10a, 11,12] Using this approach, we also synthesized coordination polymers $[Co(Cp)_2][MX_2]$ (X = $B(CN)_4$, $C(CN)_3$, $N(CN)_2$; M = K, Na) and $[Fe(Cp)_2][K\{C(CN)_3\}_2]$, shown in Figure 2b, the latter being a paramagnetic coordination polymer.

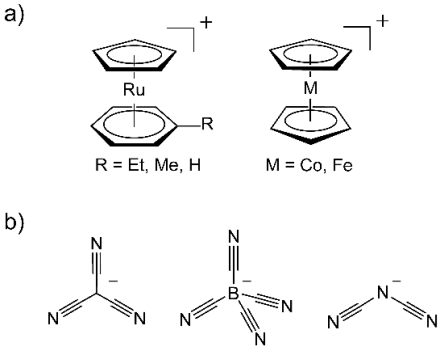

Figure 1. The structural formulas of the (a) cationic sandwich complexes and (b) polycyano anions used in this study.

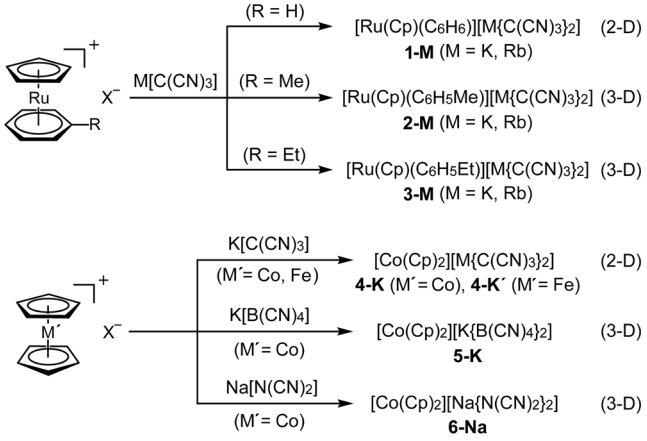

Figure 2. Synthetic schemes of coordination polymers containing (a) $[Ru(Cp)(C_6H_5R)]X$ (R = H, Me, Et) and (b) $[M(Cp)_2]X$ (M = Co, Fe) (X = Cl or $C(CN)_3$). Dimensionalities of the coordination polymers are shown in parentheses.

Result and Discussion

Preparation and General Structural Features

Figure 2a depicts the synthetic schemes for **1**–**M**, **2**–**M**, and **3**–**M** (M = K, Rb), which contain cationic ruthenium complexes. The reaction of [Ru(Cp)(C_6H_5R)]Cl and M[$C(CN)_3$] in water produced the salts in yields of 10–20%. As described in the next section, the CN groups of the anions coordinate with the alkali metal ions to form an anionic $[MX_2]_n^{n-}$ coordination polymer framework (X = $C(CN)_3^-$), which accommodates the organometallic cations. The dimensionality of the coordination framework depends on the size of the organometallic cations; **1–M** has a 2–D network structure, whereas **2–M** and **3–M** containing larger cations have 3–D network structures. By using the same method, we also synthesized coordination polymers with other cations and polycyano anions (Figure 2b), **4′**–**K** being a paramagnetic coordination polymer (Figure S1, Supporting information). They have either 2–D network structures (**4**–**K** and **4′**–**K**) or 3–D network structures (**5**–**K** and **6**–**Na**).

It is noteworthy that the coordination polymers obtained in this study are 2–D and 3–D ones, because coordination polymers that contain cationic sandwich complexes have 3–D structures[13] with very few exceptions.[14] Coordination polymers containing $C(CN)_3$ bridging ligands are usually 3–D coordination polymers.[15]

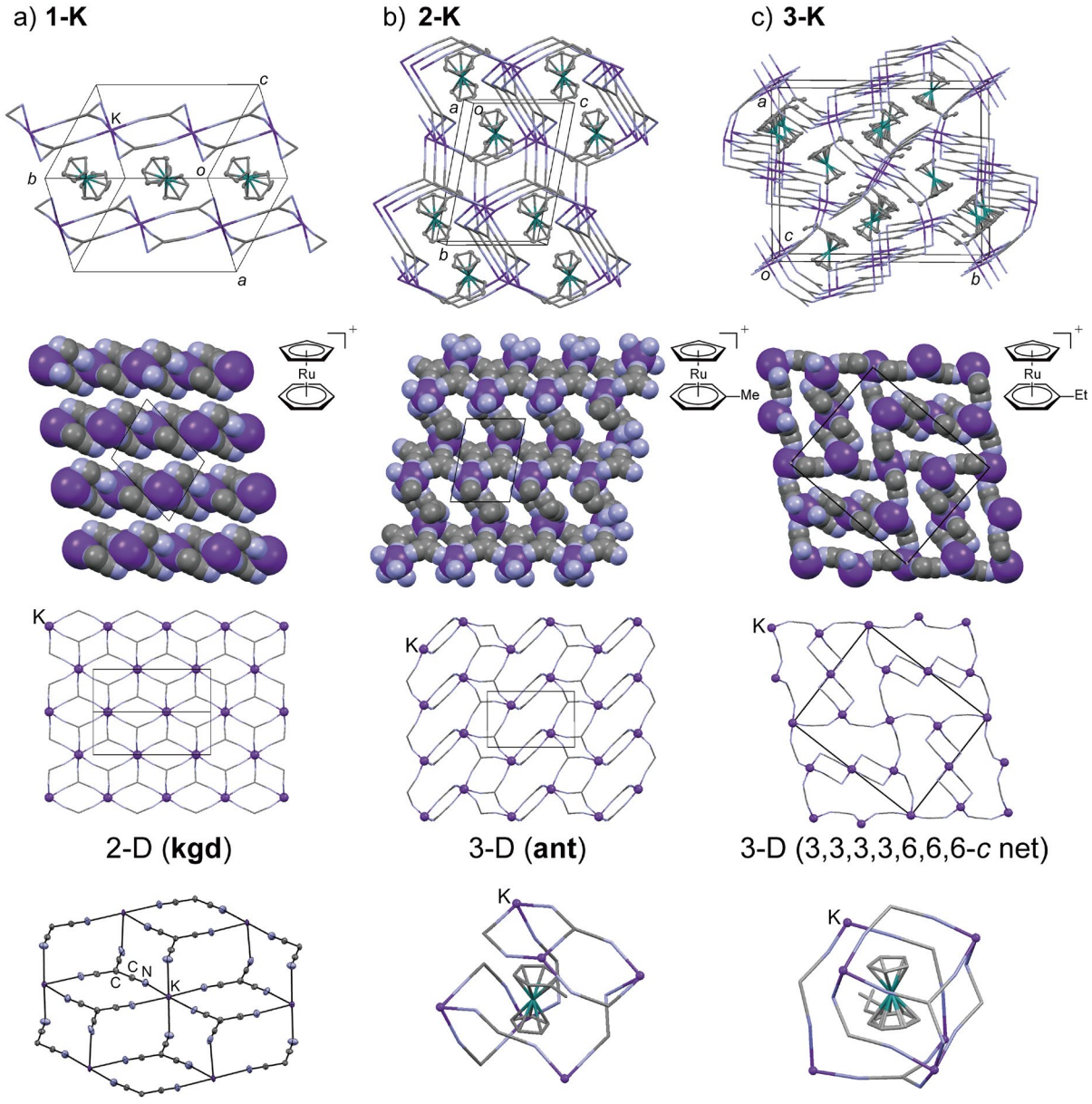

Figure 3. Crystal structures of (a) [Ru(Cp)(C_6H_6)][K{$C(CN)_2$}$_2$] (**1**–**K**), (b) [Ru(Cp)(C_6H_5Me)][K{$C(CN)_2$}$_2$] (**2**–**K**), and (c) [Ru(Cp)(C_6H_5Et)][K{$C(CN)_2$}$_2$] (**3**–**K**). Packing diagrams (top), coordination polymer structures (upper middle, cations omitted), topologies of coordination polymer frameworks (lower middle), and structures of the coordination plane/cage (bottom). The packing diagrams in (b) and (c) are viewed along the channel direction.

Crystal Structures of Ru-containing Coordination Polymers

1–**M** were 2–D coordination polymers, whereas **2**–**M** and **3**–**M** were 3–D coordination polymers. The alkali metal ion in the coordination framework has a six-coordinate octahedral coordination environment with typical coordination distances (K···N distances: 2.76–2.97 Å, Rb···N distances: 2.92–3.11 Å),[15] while the topological flexibility enabled the accommodation of various organometallic cations.

1–**K** and **1**–**Rb** possess a sheet-like 2–D coordination polymer structure, and the cationic sandwich compounds were located between the sheets. Their space groups were $P2_1/n$ and $C2/m$, respectively. The packing diagram, coordination polymer structures, and topology of **1**–**K** are shown in Figure 3a. The coordination framework has a winding 2–D sheet structure (Figure 3a, bottom), the topology of which is **kgd**.[16] The cation molecule exhibits rotational disorder at the Cp and C_6H_6 rings. The structure of **1**–**Rb** is similar to that of **1**–**K** (Figure S1a, Supporging information), though the cation molecule in **1**–**Rb** exhibits extensive disorder and the *b*-axis length is half that of **1**–**K**. The distances between the coordination polymer sheets for **1**–**K** and **1**–**Rb** were 8.37 Å and 8.19 Å, respectively. Since the contained cation molecules were the same, it is reasonable that a larger metal ionic radius results in a larger sheet size and, hence, smaller interlayer distances.

The 3–D coordination polymers, **2**–**M** and **3**–**M** (M = K, Rb), crystallized in space groups *P*–1 and *P*bam, respectively. The packing diagrams, coordination polymer frameworks, and topologies of **2**–**K** and **3**–**K** are shown in Figures 3b and 3c. They have different network topologies, **ant** and 3,3,3,3,6,6,6-*c* net, respectively. Both possess 1–D channel structures, running along the *a*- and *c*-axes, respectively. All $[C(CN)_3]$ planes were parallel to the *c*-axis in **3**–**K**, whereas **2**–**K** has a low-symmetry framework structure with a deformed octahedral coordination environment around the potassium ion. The coordination polymers have a cage-like local structure accommodating the organometallic cation (Figure 3, bottom), which are open cages formed by six potassium ions and seven bridging ligands. The cation molecule in **3**–**K** exhibited two-fold disorder at the ethyl group. The structure of **2**–**Rb** was similar to that of **2**–**K**, as shown in Figure S1b (Supporting information).

Crystal Structures of Other Coordination Polymers

The coordination polymers containing $[M(Cp)_2]$ (M = Co, Fe) and polycyano anions $C(CN)_3$, $B(CN)_4$, and $N(CN)_2$ (Figure 2b) were anionic coordination polymers similar to those containing the Ru sandwich complexes.

4–**K** was a 2–D coordination polymer (space group $C2/m$), featuring a very similar structure to that of **1**–**Rb** (Figure S1c, Supporting information), which is reasonable considering the comparable sizes of the cation molecules. The interlayer distance of **4**–**K** was 7.93 Å, which is 0.44 Å shorter than that of **1**–**K** (8.37 Å) owing to the smaller cation size. The paramagnetic coordination polymer, **4′**–**K**, containing a ferrocenium cation, was isomorphous with **4**–**K**.

5–**K** and **6**–**Na**, containing $B(CN)_4$ and $N(CN)_2$, respectively, were 3–D coordination polymers. The coordination environments of the alkali ions are different from those in coordination polymers containing $C(CN)_3$. The structure of **5**–**K** (space group $C2/c$) is shown in Figure 4. The potassium ion has an eight-coordinate, distorted square antiprismatic coordination environment (Figure 8b), in which the K–N distances (2.85–3.13 Å) were typical values.[15a] The topology of the coordination polymer framework was **flu**. The coordination network has a cage structure that accommodates the organometallic cation, as shown in Figure 8c. The coordination cage had an octahedron structure composed of six potassium ions and eight bridging ligands. One of the two crystallographically independent cation molecules exhibited rotational disorder at the Cp rings. This complex displayed a phase transition in the solid state at −15.3 °C (ΔS = 19.4 J mol^{-1} K^{-1}), which is likely associated with the rotation of the cation molecule, given the large transition entropy. On the other hand, **6**–**Na** ($C2/c$ space group) had a more complicated coordination structure. The packing diagram of the complex is shown in Figure S1d (Supporting information). The sodium ion has a six-coordinate structure, forming a trinuclear unit via μ^2 coordination of the CN groups, and the unit was further connected to form a network structure. Since the data quality was not sufficient, we refrain from discussing its structure in detail.

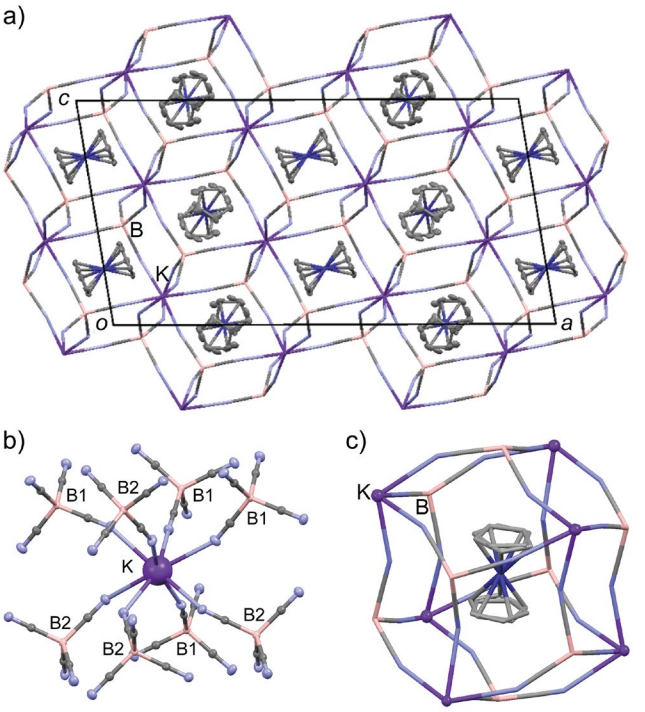

Figure 4. Crystal structure of $[Co(Cp)_2][K\{B(CN)_4\}_2]$ (**5**–**K**). (a) Packing diagram, (b) coordination environment around the potassium ion, and (c) coordination cage accommodating the guest.

Thermal Properties of Coordination Polymers

The coordination polymers melted or displayed incongruent melting behavior at high temperatures. Their thermal properties were investigated using differential scanning calorimetry (DSC). The melting points and melting entropies are shown in Table 1, and the DSC chart is shown in Figure S3 (Supporting information). In addition, a solid phase transition was observed with **2**–**K** at 107.8 °C (ΔS = 28.2 J mol^{-1} K^{-1}).

The melting points of the Ru-containing coordination polymers are compared in Figure 5a. The melting points decreased with increasing metal ion radius (radius: K < Rb) and elongation of the cation molecule substituent (melting point: **1-M** > **2-M** > **3-M**). The metal ion dependence is reasonable because the smaller radius of K^+ compared to Rb^+ brings about the larger lattice energy of the K salt. **1**–**K**, with the highest melting point (T_m = 239.3 °C), decomposed immediately after melting, whereas **1**–**Rb** and **2**–**Rb** (T_m = 204.8 and 149.0 °C) gradually turned yellow after melting, indicating gradual decomposition in the liquid state. Optical microscopy images of the melting and crystallization of **2**–**Rb** are shown in Figure 6a. On the other hand, **2**–**K**, **3**–**K**, and **3**–**Rb** exhibited incongruent melting behaviors at T_m = 214.6, 132.9, and 102.9 °C, respectively (striped bars in Figure 5a), at which a phase separation occurred concomitantly, as discussed in detail in the next section. To investigate the decomposition behaviors, thermogravimetric (TG) analyses were performed on **1**–**K**, **2**–**K**, **3**–**K**, and **1**–**Rb** (Figure S4, Supporting information). Their decomposition temperatures (−5wt%) were 239, 228, 217, and 223 °C, respectively. The results are consistent with the microscope observation. The decomposition of **1**–**K** occurred immediately after melting, whereas other compounds exhibited weight loss above their melting points at around 220 °C. It should be noted that gradual coloration of the liquid occurred in the latter cases even below 200 °C, indicating that degradation by chemical reaction occurs before the weight loss occurs.

On the other hand, **4**–**K**, **5**–**K** and **6**–**Na** exhibited higher melting points and decomposed upon melting (Figure 5b). Their melting points decreased in the order **5**–**K** (T_m = 373 °C) > **4**–**K** (T_m = 244 °C) > **6**–**Na** (T_m = 167 °C); these compounds respectively contained $B(CN)_4$, $C(CN)_3$, and $N(CN)_2$. This melting point trend is the same as that observed in the potassium salts of the polycyano anions (Table 1), in which the melting points decreased with decreasing number of polycyano groups involved in the coordination bonds. **4**–**K** decomposed immediately upon melting, though melting and crystallization of **5**–**K** gradually turned irreversible owing to the higher thermal stability of $B(CN)_4$.[9] On the other hand, **6**–**Na** exhibited incongruent melting behavior and decomposed immediately afterward. The paramagnetic complex, **4′**–**K**, decomposed without melting at approximately 310 °C.

These observations indicated that the melting behaviors of the coordination polymers vary depending on their components. While the melting of high-melting-point complexes was associated with thermal decomposition, low-melting-point complexes had a tendency to undergo incongruent melting with less thermal decomposition.

Table 1. Melting points and melting entropies of coordination polymers, ionic liquids, and metal salts.

Compound	Melting point (°C)	ΔS (J mol^{-1} K^{-1})
Coordination polymers		
1–**K**	239.3[d]	51.7
1–**Rb**	204.8	86.3
2–**K**	214.6[c]	44.7
2–**Rb**	149.0	41.8
3–**K**	132.9[c]	87.5
3–**Rb**	102.9[c]	60.7
4–**K**	244.0[d]	125.8
5–**K**[a]	373[d]	
6–**Na**[a]	167[c]	
Ionic liquids		
$[Ru(Cp)(C_6H_6)][C(CN)_3]$[b]	90.2	27.5
$[Ru(Cp)(C_6H_5CH_3)][C(CN)_3]$[b]	−1.3	73.7
$[Ru(Cp)(C_6H_5C_2H_5)][C(CN)_3]$[b]	−86 (T_g)	—
Metal salts		
$Na[C(CN)_3]$[a]	(>367)	
$K[C(CN)_3]$[a]	289	
$Rb[C(CN)_3]$	225.3	43.0
$K[B(CN)_4]$[a]	413	

[a]Visual observation. [b]Ref. 9. [c]Incongruent melting. [d]Decomposed immediately after melting.

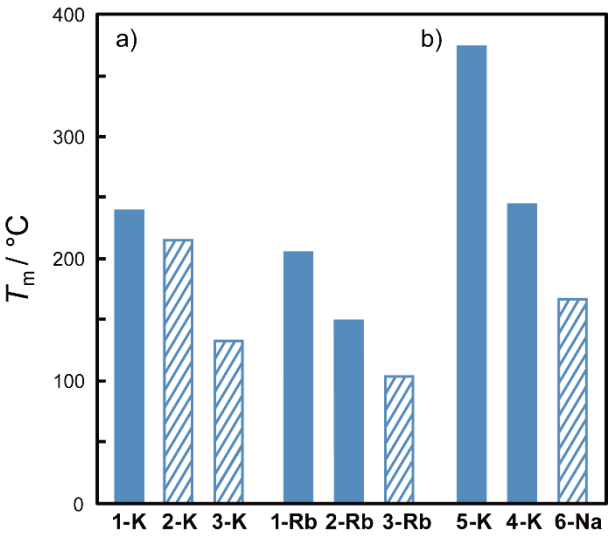

Figure 5. Melting points of coordination polymers containing the (a) Ru and (b) Co complexes. The coordination polymers that undergo incongruent melting are shown by the striped bars.

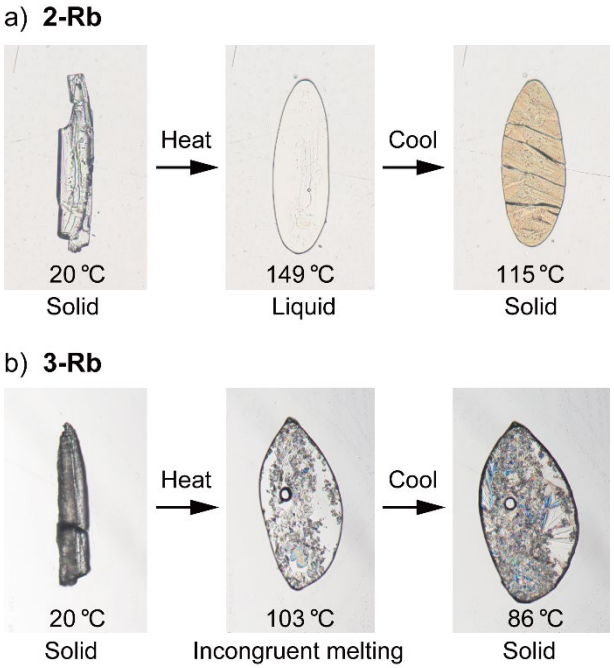

Figure 6. Polarizing optical microscopy images of melting and crystallization of (a) $[Ru(Cp)(C_6H_5CH_3)][Rb\{C(CN)_3\}_2]$ (**2**–**Rb**) and (b) $[Ru(Cp)(C_6H_5C_2H_5)][Rb\{C(CN)_3\}_2]$ (**3**–**Rb**).

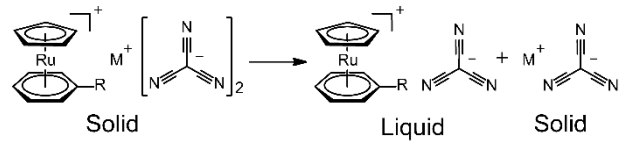

Figure 7. Scheme of disproportionation reaction accompanying incongruent melting of the coordination polymer.

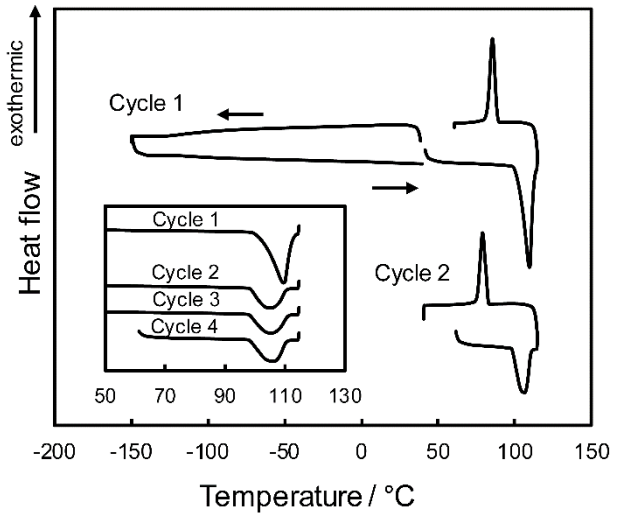

Figure 8. DSC traces of $[Ru(Cp)(C_6H_5C_2H_5)][Rb\{C(CN)_3\}_2]$ (**3**–**Rb**). Inset displays the results of repeated measurements recorded upon heating.

Incongruent Melting Behavior

As shown in the previous section, **3**–**K**, **3**–**Rb**, and **2**–**K** exhibited incongruent melting behavior, displaying phase separation upon melting. Incongruent melting has been observed in silicate minerals, metal salts, and molecular compounds,[17] though very few examples of incongruent melting of coordination polymers have been reported.[18]

Microscope images depicting the melting behaviors of **3**–**Rb** and **3**–**K** are shown in Figure 6b and Figure S5 (Supporting information), respectively. Upon melting, disproportionation occurred, as illustrated in Figure 7, giving a mixture of solid $M[C(CN)_3]$ and ionic liquid $[Ru(Cp)(C_6H_5R)][C(CN)_3]$ containing a small amount of dissolved $M[C(CN)_3]$, as confirmed by X-ray diffraction experiments (Figure S6, Supporting information). When the mixture was cooled, part of the liquid phase underwent peritectic formation, and subsequent cycles reversibly switched between melting and crystallization. The liquid phase did not decompose in the case of **3**–**Rb** (T_m = 102.9 °C) in these cycles. However, gradual decomposition of the ionic liquid component was observed when **3**–**K** melted (T_m = 132.9 °C), gradually turning yellow. A higher extent of thermal decomposition was observed for **2**–**K** (T_m = 214.6 °C) after melting, along with low reversibility in the melting-crystallization process. When **3**–**Rb** was further heated above the incongruent melting point, complete dissolution of $M[C(CN)_3]$ was observed at approximately 220 °C, though it accompanied gradual decomposition of the liquid phase (Figure S7, Supporting information).

The incongruent melting behaviors of these salts were investigated using DSC. The DSC traces of **3**–**Rb** are shown in Figure 8. The incongruent melting was observed as an endothermic peak upon the initial heating (102.9 °C, ΔH = 23.2 kJ mol^{-1}), and in the subsequent cycles, reversible crystallization and melting of the coordination polymer component was observed (T_m = 99 °C, ΔH = 13 kJ mol^{-1}). The enthalpy values indicate that roughly half of the coordination polymers reversibly melted and solidified, which indicates that half of the $Rb[C(CN)_3]$ component precipitated during the initial incongruent melting and half of the ionic liquid component remained as liquid even at room temperature. The glass transition of the remaining ionic liquid component was consistently observed at −85 °C in the DSC cycles after the incongruent melting.[9] These observations were consistent with the microscope observations. **3**–**K** exhibited almost the same melting behavior. Upon heating, incongruent melting was detected at 132.9 °C (ΔH = 35.8 kJ mol^{-1}), crystallization was observed upon cooling, and subsequent heating resulted in melting at 127 °C (ΔH = 21 kJ mol^{-1}). Since **3**–**K** had a higher melting point than **3**–**Rb**, a slower scanning speed (5 °C min^{-1}) resulted in slight decomposition of the liquid phase, which was observed as a gradual decrease of the melting point and melting enthalpy in subsequent cycles (Figure S8, Supporting information).

The incongruent melting phenomenon observed in these salts is ascribed to the low solubility of $M[C(CN)_3]$ in the ionic liquid phase at the melting temperature. This also explains the incongruent melting behavior of **2**–**K** (T_m = 214.6 °C) despite its higher melting point than that of **2**–**Rb**, which undergoes normal

melting (T_m = 149.0 °C). This phenomenon, which resulted from the lower solubility of K[C(CN)$_3$] than that of Rb[C(CN)$_3$] in the ionic liquid phase, is consistent with the smaller ionic radius of the potassium ion. The smaller ionic radius brings about the larger lattice energy as reflected in the higher melting point of K[C(CN)$_3$] (Table 1).

Conclusions

In this study, we synthesized a series of 2–D and 3–D anionic coordination polymers that accommodate organometallic cations as guests inside their coordination frameworks and that melt or exhibit incongruent melting phenomena. The incongruent melting phenomenon has rarely been reported in coordination polymers. The material design of these melting coordination polymers is based on the formation of complex salts from an organometallic ionic liquid and a polycyano anion, in which the polycyano anion acts as both the counter anion of the ionic liquids and bridging ligands of the coordination polymers. We demonstrated that various polycyano anions, metal ions, and organometallic cations can be used to construct them, and this leads to different coordination structures, framework dimensionalities, melting behaviors, and even magnetic properties. The next goal is to improve their thermal stabilities to achieve fully reversible melting phenomena towards being used for melt-quenching or other processing methods. Thus, we are currently synthesizing related coordination polymers using components that are more thermally stable.

Experimental Section

General

[Ru(Cp)(C$_6$H$_5$R)][PF$_6$] (R = H, Me, Et)[19] and [Ru(Cp)(C$_6$H$_6$)][C(CN)$_3$][9] were prepared according to literature methods. [Ru(Cp)(C$_6$H$_5$R)]Cl were produced from the corresponding PF_6 salts using anion exchange resin (Dowex 1X8, Cl form, eluent: methanol).[9] Rb[C(CN)$_3$] and Na[C(CN)$_3$] were prepared through cation exchange from K[C(CN)$_3$] using cation exchange resin (Amberite IR120). DSC measurements were performed using a TA Instruments Q100 differential scanning calorimeter at a rate of 10 K min^{-1}. Themogravimetric analyses were performed using a Rigaku TG8120 at 10 K min^{-1} under nitrogen. Infrared (IR) spectra were recorded via attenuated total reflectance (ATR diamond) using a Thermo Scientific Nicolet iS 5 FT-IR spectrometer. Electrospray ionization-mass spectrometry spectra were recorded using a Thermo Fisher Scientific LTQ Orbitrap Discovery system. Powder X-ray diffraction measurements were performed using a Bruker APEX II Ultra.

Preparation of coordination polymers containing [Ru(Cp)(C$_6$H$_5$R)]

[Ru(Cp)(C$_6$H$_6$)][K{C(CN)$_3$}$_2$] (1–K). An aqueous solution (0.2 mL) of K[C(CN)$_3$] (28 mg, 0.22 mmol) was added to an aqueous solution (0.3 mL) of [Ru(Cp)(C$_6$H$_6$)][C(CN)$_3$] (55 mg, 0.17 mmol). The mixture was stirred for 15 min and filtered, and the filtrate was evaporated under reduced pressure. Recrystallization of the crude product from acetone-diethyl ether (−40 °C) gave the desired product as pale yellow block crystals (9 mg, yield 12%). Anal. Calcd. for C$_{19}$H$_{11}$N$_6$KRu: C, 49.24; H, 2.39; N, 18.13. Found: C, 49.34; H, 1.86; N, 18.04. IR (cm^{-1}): 3085, 2158 (CN), 1446, 1233, 1108, 981, 916, 854, 826, 565. This compound was also prepared via the reaction of [Ru(Cp)(C$_6$H$_6$)]Cl and K[C(CN)$_3$] in water.

[Ru(Cp)(C$_6$H$_6$)][Rb{C(CN)$_3$}$_2$] (1–Rb). An aqueous solution (0.1 mL) of Rb[C(CN)$_3$] (62 mg, 0.35 mmol) was added to an aqueous solution (0.1 mL) of [Ru(Cp)(C$_6$H$_6$)]Cl (0.16 mmol). The mixture was stirred for 15 min and filtered, and the filtrate was evaporated under reduced pressure. Recrystallization of the solid from acetonitrile-diethyl ether (−40 °C) gave the desired product as pale yellow needle crystals (51 mg, yield 21%). Anal. Calcd. for C$_{19}$H$_{11}$N$_6$RbRu: C, 44.76; H, 2.17; N, 16.48. Found: C, 45.07; H, 1.51; N, 16.51. IR (cm^{-1}): 2156, 1445, 1415, 1231, 1004, 851, 823, 563.

[Ru(Cp)(C$_6$H$_5$CH$_3$)][K{C(CN)$_3$}$_2$] (2–K). This compound was prepared as described for **1**–**Rb** using [Ru(Cp)(C$_6$H$_5$CH$_3$)]Cl and K[C(CN)$_3$]. Recrystallization of the crude product from acetone-diethyl ether (−40 °C) gave the desired product as pale yellow plate crystals (29 mg, yield 20%). Anal. Calcd. for C$_{20}$H$_{13}$N$_6$KRu: C, 50.30; H, 2.74; N, 17.60. Found: C, 50.40; H, 2.53; N, 17.55. IR (cm^{-1}): 2162 (CN), 1455, 1414, 1384, 1234, 1150, 1108, 1041, 1003, 856, 564.

[Ru(Cp)(C$_6$H$_5$CH$_3$)][Rb{C(CN)$_3$}$_2$] (2–Rb). This compound was prepared as described for **1**–**Rb** using [Ru(Cp)(C$_6$H$_5$CH$_3$)]Cl and Rb[C(CN)$_3$]. Recrystallization of the crude product from ethanol (−40 °C) gave the desired product as pale yellow needle crystals (26 mg, yield 21%). Anal. Calcd. for C$_{20}$H$_{13}$N$_6$RbRu: C, 45.85; H, 2.50; N, 16.04. Found: C, 46.04; H, 2.18; N, 16.01. IR (cm^{-1}): 3112, 2160 (CN), 1456, 1414, 1387, 1232, 1041, 1004, 850, 562, 528.

[Ru(Cp)(C$_6$H$_5$C$_2$H$_5$)][K{C(CN)$_3$}$_2$] (3–K). This compound was prepared as described for **1**–**Rb** using [Ru(Cp)(C$_6$H$_5$C$_2$H$_5$)]Cl (0.23 mmol) and K[C(CN)$_3$] (65 mg, 0.50 mmol). Recrystallization of the crude product from acetone-diethyl ether (−40 °C) gave the desired product as pale yellow needle crystals (11 mg, yield 12%). Anal. Calcd. for C$_{21}$H$_{15}$N$_6$KRu: C, 51.31; H, 3.08; N, 17.10. Found: C, 51.29; H, 2.88; N, 16.78. IR (cm^{-1}): 3112, 2977, 2160 (CN), 1530, 1457, 1414, 1237, 1146, 1107, 1003, 974, 851, 781, 761, 565.

[Ru(Cp)(C$_6$H$_5$C$_2$H$_5$)][Rb{C(CN)$_3$}$_2$] (3–Rb). An aqueous solution (0.1 mL) of Rb[C(CN)$_3$] (56 mg, 0.32 mmol) was added to an aqueous solution (0.1 mL) of [Ru(Cp)(C$_6$H$_5$C$_2$H$_5$)]Cl (0.09 mmol). The mixture was stirred for 30 min at 8 °C and the precipitate was collected by filtration. Recrystallization of the solid from ethanol (−40 °C) gave the desired product as pale yellow needle crystals (8 mg, yield 16%). Anal. Calcd. for C$_{21}$H$_{15}$N$_6$RbRu: C, 46.89; H, 2.81; N, 15.62. Found: C, 47.05; H, 2.88; N, 15.52. IR (cm^{-1}): 2359, 2161 (CN), 1458, 1414, 1238, 1003, 850, 565.

Preparation of coordination polymers containing [M(Cp)$_2$]

[Co(Cp)$_2$][K{C(CN)$_3$}$_2$] (4–K). This compound was prepared as described for **1**–**Rb** using [Co(Cp)$_2$]Cl and K[C(CN)$_3$]. The desired product was obtained as orange block crystals (22 mg, yield 18%). Anal. Calcd. for C$_{18}$H$_{10}$N$_6$KCo: C, 52.94; H, 2.47; N, 20.58. Found: C, 53.11; H, 2.30; N, 20.55. IR (cm^{-1}): 3119, 2160 (CN), 1414, 1233, 1008, 888, 860, 564.

[Fe(Cp)$_2$][K{C(CN)$_3$}$_2$] (4′–K). This compound was prepared as described for **1**–**Rb** using [Fe(Cp)$_2$]Cl and K[C(CN)$_3$]. The desired product was obtained as fine blue crystals (31 mg, yield 50%). Anal. Calcd. for C$_{18}$H$_{10}$N$_6$KFe: C, 53.35; H, 2.49; N, 20.74. Found: C, 52.67; H, 1.62; N, 20.38. IR (cm^{-1}): 3116, 2160, 1417, 1234, 1010, 851, 564, 545, 527.

[Co(Cp)$_2$][K{B(CN)$_4$}$_2$] (5–K). This compound was prepared as described for **1**–**Rb** using [Co(Cp)$_2$]Cl and K[B(CN)$_4$]. The product was obtained through slow evaporation of an acetone solution over three days as yellow

block crystals (16 mg, yield 12%). Anal. Calcd. for $C_{18}H_{10}N_8B_2KCo$: C, 47.21; H, 2.20; N, 24.47. Found: C, 47.20; H, 1.74; N, 24.53. IR (cm^{-1}): 3119, 2228, 967, 932, 864.

$[Co(Cp)_2][Na\{N(CN)_2\}_2]$ (6–Na). $[Co(Cp)_2][N(CN)_2]$ was synthesized via the metathesis of $[Co(Cp)_2]Cl$ (44 mg, 0.19 mmol) and $Na[N(CN)_2]$ (43 mg, 0.49 mmol) in water-dichloromethane. After an equivalent amount of $Na[N(CN)_2]$ was added, the mixture was ground with an agate mortar and pestle and dissolved in acetonitrile and filtered. Slow evaporation of the solution in a desiccator under reduced pressure gave the desired product as orange block crystals in two days (1.4 mg, yield 2%). High-resolution mass spectrometry (HRMS) *m/z* calcd. for $[C_{10}H_{10}Co]^+$: 189.0115. Found: 189.0103. Calcd. for $[C_2N_3]^-$: 66.0092. Found: 66.0103.

X-ray crystallography

The crystal structures of **1**–**K**, **1**–**Rb**, **2**–**K**, **2**–**Rb**, **3**–**K**, **4**–**K**, and **5**–**K** were determined using X-ray crystallography at 100 K. The diffraction data were collected using a Bruker APEX II Ultra CCD diffractometer with MoKα radiation (λ = 0.71073 Å). The structures were solved using the direct method using SHELXL.[20] The molecular structures and packing diagrams were drawn using Mercury [21]. The crystallographic parameters are shown in Tables S1–S2 (Supporting information). We also tried to determine the crystal structure of **6**–**Na**, but the refinements were unsatisfactory because of severe twinning. CCDC 1852055 (1-K), 1862692 (**1-Rb**), 1852014 (**2-K**), 1849258 (**2-Rb**), 1862763 (**3-K**), 1852070 (**4-K**), and 1851507 (**5-K**) contain the supplementary crystallographic data for this paper. These data are provided free of charge by The Cambridge Crystallographic Data Centre.

Acknowledgements

We thank Dr. Yusuke Funasako (Sanyo-Onoda City University) for his help with X-ray structure determination and Ryo Sumitani for TG measurements. This work was supported financially by KAKENHI (18H04516 and 16H04132) from the Japan Society for the Promotion of Science (JSPS).

Keywords: coordination polymers • sandwich complexes • crystal structures • thermal properties

[1] a) S. Kitagawa, *Acc. Chem. Res.* **2017**, *50*, 514–516; b) H. Furukawa, K. E. Cordova, M. O'Keeffe, O. M. Yaghi, Science, **2013**, *341*, 1230444; c) G. K. Kole, J. J. Vittal, *Chem. Soc. Rev.* **2013**, 42, 1755–1775.

[2] T. D. Bennett, S. Horike, *Nat. Rev. Mater.* **2018**, *3*, 431–440.

[3] a) E. T. Spielberg, E. Edengeiser, B. Mallick, M. Havenith, A. Mudring, *Chem. Eur. J.* **2014**, *20*, 5338–5345; b) M. Moriya, D. Kato, W. Sakamoto, T. Yogo, *Chem. Eur. J.* **2013**, *19*, 13554–13560; c) Y. Hirai, T. Nakanishi, Y. Kitagawa, K. Fushimi, T. Seki, H. Ito, H. Fueno, K. Tanaka, T. Satoh, Y. Hasegawa, *Inorg. Chem.* **2015**, *54*, 4364–4370; d) Y. Su, Y. Cui, Y. Wang, R. Lin, W. Zhang, J. Zhang, X. Chen, *Cryst. Growth. Des.* **2015**, *15*, 1735–1739; e) D. Depuydt, N. R. Brooks, S. Schaltin, L. Van Meervelt, J. Fransaer, K. Binnemans, *ChemPlusChem* **2013**, *78*, 578–588.

[4] a) D. Umeyama, S. Horike, M. Inukai, T. Itakura, S. Kitagawa, *J. Am. Chem. Soc.* **2015**, *137*, 864–870; b) D. Umeyama, N. P. Funnell, M. J. Cliffe, J. A. Hill, A. L. Goodwin, Y. Hijikata, T. Itakura, T. Okubo, S. Horike, S. Kitagawa, *Chem. Commun.* **2015**, *51*, 12728–12731; c) W. Q. Chen, S. Horike, D. Umeyama, N. Ogiwara, T. Itakura, C. Tassel, Y. Goto, H. Kageyama, S. Kitagawa, *Angew. Chem. Int. Ed.* **2016**, *55*, 5195–5200; d) Y. Ohara, A. Hinokimoto, W. Q. Chen, T. Kitao, Y. Nishiyama, Y. L. Hong, S. Kitagawa, S. Horike, *Chem. Commun.* **2018**, *54*, 6859–6862.

[5] a) T. D. Bennett, J. Tan, Y. Yue, E. Baxter, C. Ducati, N. J. Terrill, H. H. Yeung, Z. Zhou, W. Chen, S. Henke, A. K. Cheetham, G. N. Greaves, *Nat. Commun.* **2015**, *6*, 1–7; b) R. Gaillac, P. Pullumbi, K. A. Beyer, K. W. Chapman, D. A. Keen, T. D. Bennett, F. X. Coudert, *Nat. Mater.* **2017**, *16*, 1149–1154; c) T. D. Bennett, Y. Z. Yue, P. Li, A. Qiao, H. Z. Tao, N. G. Greaves, T. Richards, G. I. Lampronti, S. A. T. Redfern, F. Blanc, O. K. Farha, J. T. Hupp, A. K. Cheetharm, D. A. Keen, *J. Am. Chem. Soc.* **2016**, *138*, 3484–3492; d) L. Longley, S.M. Collins, C. Zhou, G. J. Smales, S. E. Norman, N. J. Brownbill, C. W. Ashling, P. A. Chater, R. Tovey, C. B. Schonlieb, T. F. Headen, N. J. Terrill, Y. Z. Yue, A. J. Smith, F. Blanc, D. A. Keen, P. A. Midgley, T. D. Bennett, *Nat. Commun.* **2018**, *9*, 2135.

[6] M. Kato, H. Ito, M. Hasegawa, K. Ishii, *Chem. Eur. J.* **2019**, 2019, *25*, 5105–5112.

[7] A. Stark, K. R. Seddon, *in Kirk–Othmer Encyclopedia of Chemical Technology*, *Vol. 26*, Wiley-Interscience, New York, 5th ed., **2007**, pp. 836–919.

[8] a) T. Inagaki, T. Mochida, M. Takahashi, C. Kanadani, T. Saito, D. Kuwahara, *Chem. – Eur. J.* **2012**, *18*, 6795–6804; b) Y. Funasako, T. Inagaki, T. Mochida, T. Sakurai, H. Ohta, K. Furukawa, T. Nakamura, *Dalton Trans.* **2013**, *42*, 8317–8327; c) A. Komurasaki, Y. Funasako, T. Mochida, *Dalton Trans.* **2015**, *44*, 7595–7605.

[9] T. Tominaga, T. Ueda, T. Mochida, *Phys. Chem. Chem. Phys.* **2017**, *19*, 4352–4359.

[10] a) S. R. Batten, K. S. Murray, *Coord. Chem. Rev.* **2003**, *246*, 103–130; b) C. Nitschke, M. Köckerling, *Inorg. Chem.* **2011**, *50*, 4313–4321; c) J. A. Schlueter, J. L. Manson, U. Geiser, *Inorg. Chem.* **2005**, *44*, 3194–3202; d) D. R. Turner, A. S. R. Chesman, K. S. Murray, G. B. Deacon, S. R. Batten, *Chem. Commun.* **2011**, *47*, 10189–10210.

[11] N. R. de Tacconi, K. Rajeshwar, R. O. Lezna, *Chem. Mater.* **2003**, *15*, 3046–3062.

[12] a) T. Iwamoto, *J. Incl. Phenom. Mol. Recognit. Chem.* **1996**, *24*, 61–132; b) H. Yoshikawa, S. Nishikiori, K. Suwinska, R. Luboradzkib, J. Lipkowski, *Chem. Commun.* **2001**, 1398–1399.

[13] P. M. Van der Werff, E. Martinez-Ferrero, S. R. Batten, P. Jensen, C. Ruiz-Perez, M. Almeida, J. C. Waerenborgh, J. D. Cashion, B. Moubaraki, J. R. Galan-Mascaros, J. M. Martines-Agudo, E. Coronado, K. S. Murray, *Dalton Trans.* **2005**, 285–290.

[14] (a) M. Clemente-León, E. Coronado, J. Galán-Mascarós, C. J. Gómez-García, *Chem. Commun.* **1997**, 1727–1728. (b) E. Coronado, J. R. Galán-Mascarós, C. J. Gómez-García, J. M. Martínez-Agudo, E. Martínez-Ferrero, J. C. Waerenborgh, M. Almeida, *J. Solid State Chem.*, **2001**, *159*, 391–402.

[15] a) P. Andersen, B. Klewe, *Nature* **1963**, *200*, 464; b) O. Reckeweg, A. Schulz, F. J. Di Salvo, *Z. Naturforsch.* **2015**, *70*, 151–154.

[16] V. A. Blatov, A. P. Shevchenko, D. M. Proserpio, *Cryst. Growth. Des.* **2014**, *14*, 3576−3586.

[17] a) S. P. Chaudhuri, *Ceram. Int.* **1987**, *13*, 177–181; b) J. B. Ott, J. R. Goates, *J. Chem. Eng. Data* **1996**, *41*, 669–677.

[18] a) D. V. Soldatov, J. A. Ripmeester, *Chem. Mater.* **2000**, *12*, 1827–1839; b) F. J. M. Casado, M. R. Riesco, I. da Silva, M. I. R. Yélamos, A. Labrador, J. A. R. Cheda, *Cryst. Growth Des.*, **2011**, *11*, 759–767.

[19] F. Grepioni, G. Cojazzi, D. Braga, E. Marseglia, L. Scaccianoce, B. F.G. Johnson, *J. Chem. Soc., Dalton Trans.* **1999**, 553–558.

[20] G. M. Sheldrick, *Acta Crystallogr., Sect. A: Found. Crystallogr.* **2008**, *64*, 112–122.

[21] C. F. Macrae, I. J. Bruno, J. A. Chisholm, P. R. Edgington, P. McCabe, E. Pidcock, L. Rodriguez-Monge, R. Taylor, J. van de Streek, P. A. Wood, *J. Appl. Crystallogr.* **2008**, 41, 466–470.

Table of Contents

FULL PAPER

Melting coordination polymers: We synthesized 2–D and 3–D coordination polymers that melt or exhibit incongruent melting (T_m = 102–239 °C) and are complex salts comprising an organometallic ionic liquid and an alkali metal salt of a polycyano anion. They have anionic coordination polymer frameworks that accommodate organometallic cations as guests.

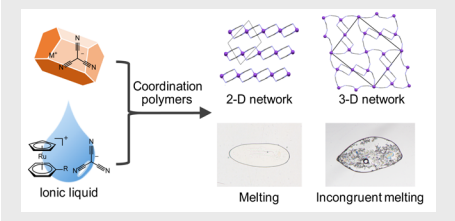

Hironori Kimata, Tomoyuki Mochida

Page No. – Page No.

Crystal Structures and Melting Behaviors of 2–D and 3–D Anionic Coordination Polymers Containing Organometallic Ionic Liquid Components

Supporting Information

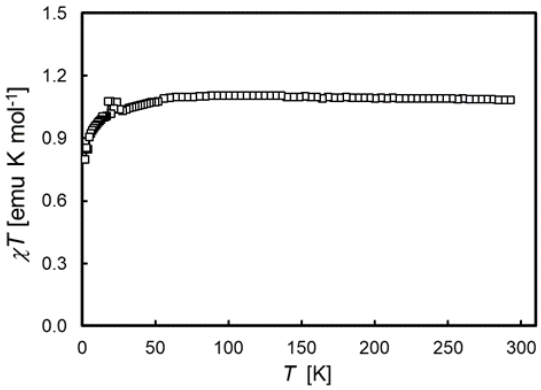

Fig. S1. Temperature dependence of the magnetic susceptibility (χT) of **4-K** measured under 1T.

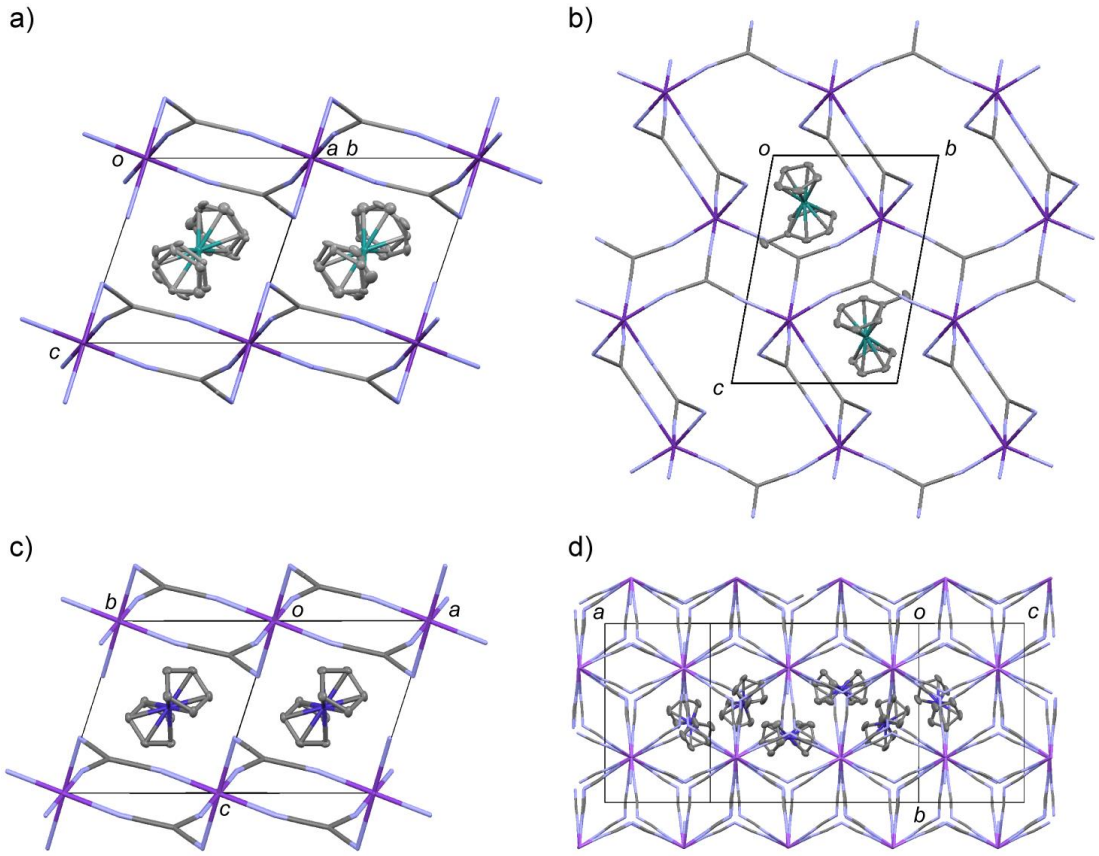

Fig. S2. Packing diagrams of (a) **1**–**Rb**, (b) **2**–**Rb**, (c) **5**–**K**, and (d) **6**–**Na**. Hydrogen atoms have been omitted for clarity.

(a) $[Ru(Cp)(C_6H_6)][K\{C(CN)_3\}_2]$ (**1**–**K**)

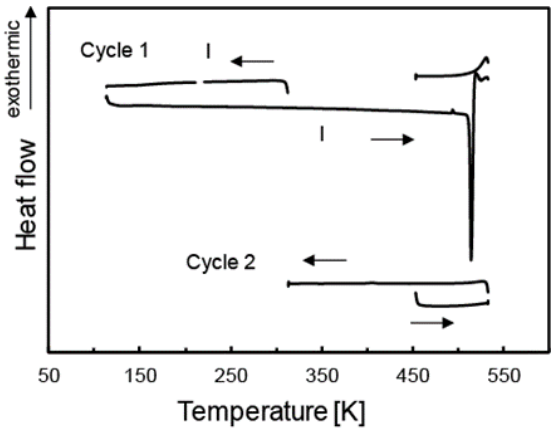

(b) $[Ru(Cp)(C_6H_6)][Rb\{C(CN)_3\}_2]$ (**1**–**Rb**)

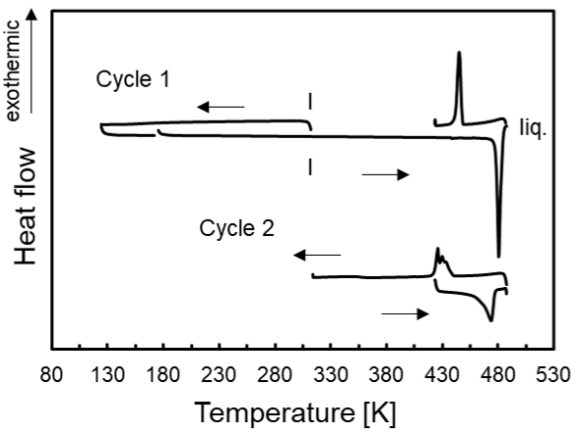

(c) $[Ru(Cp)(C_6H_5CH_3)][K\{C(CN)_3\}_2]$ (**2**–**K**)

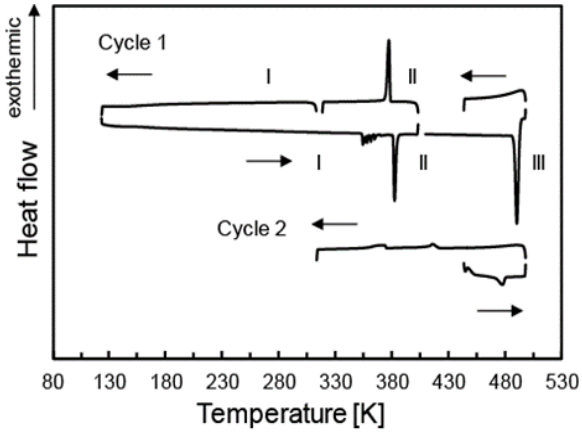

(d) $[Ru(Cp)(C_6H_5CH_3)][Rb\{C(CN)_3\}_2]$ (**2**–**Rb**)

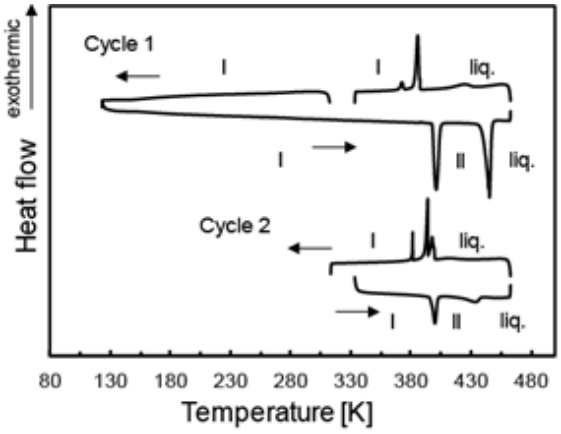

(e) $[Ru(Cp)(C_6H_5C_2H_5)][K\{C(CN)_3\}_2]$ (**3**–**K**)

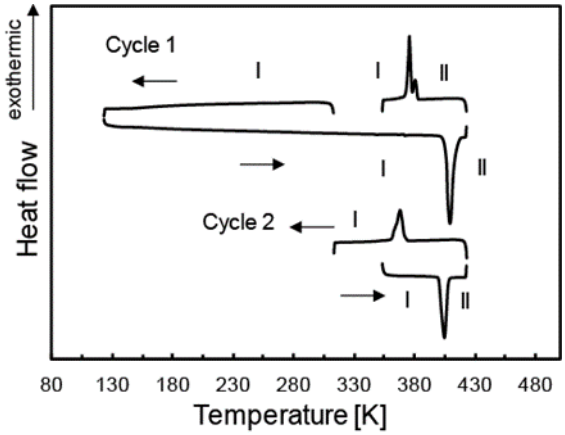

(f) $[Ru(Cp)(C_6H_5C_2H_5)][Rb\{C(CN)_3\}_2]$ (**3**–**Rb**)

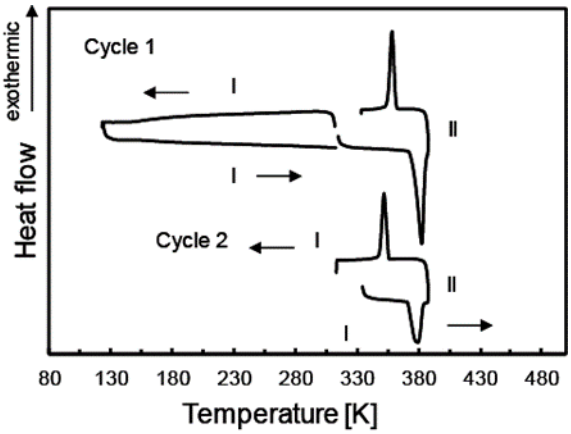

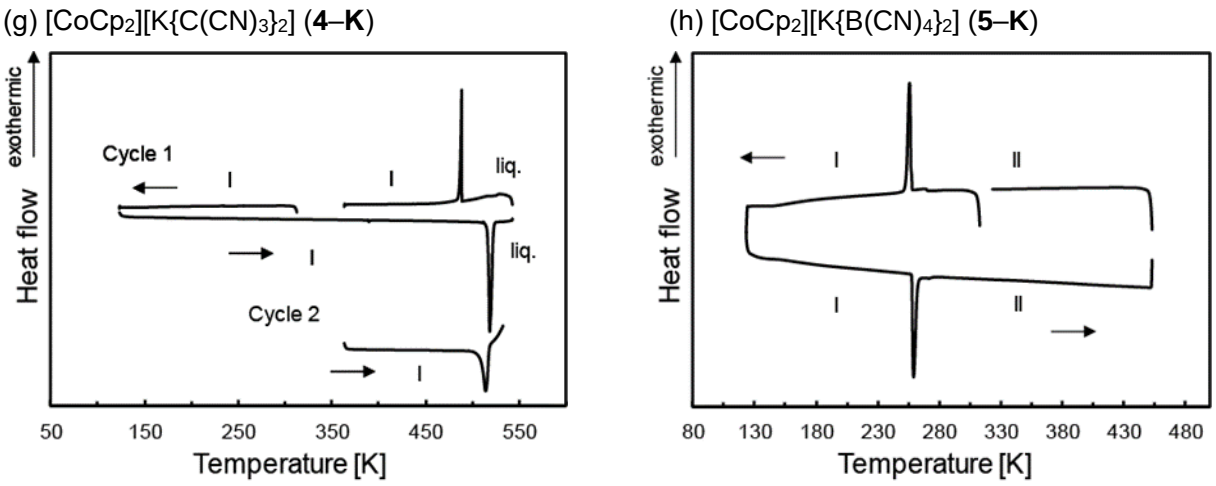

Fig. S3. DSC traces of (a) **1**–**K**, (b) **1**–**Rb**, (c) **2**–**K**, (d) **2**–**Rb**, (e) **3**–**K**, (f) **3**–**Rb**, (g) **4**–**K**, and (h) **5**–**K**.

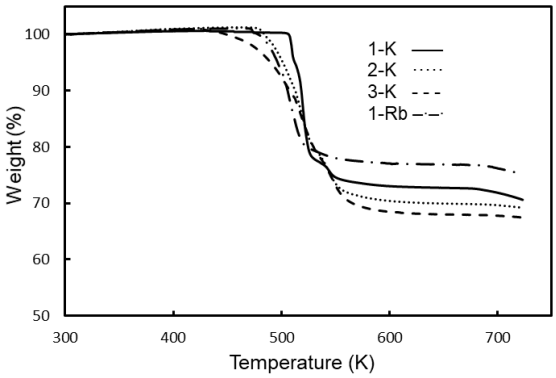

Fig. S4. TG traces of **1-K**, **2-K**, **3-K** and **1-Rb** (scan rate: 10 $Kmin^{-1}$).

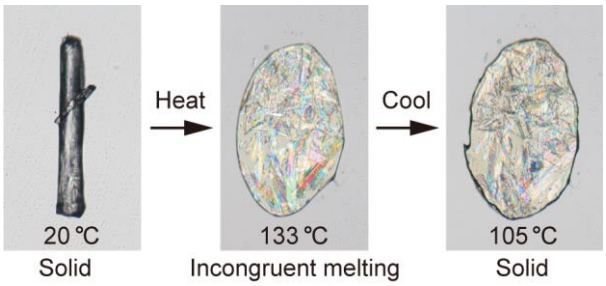

Fig. S5. Polarized micrographs of incongruent melting process of [Ru(Cp)($C_6H_5C_2H_5$)][K{C(CN)$_3$}$_2$] (**3**–**K**).

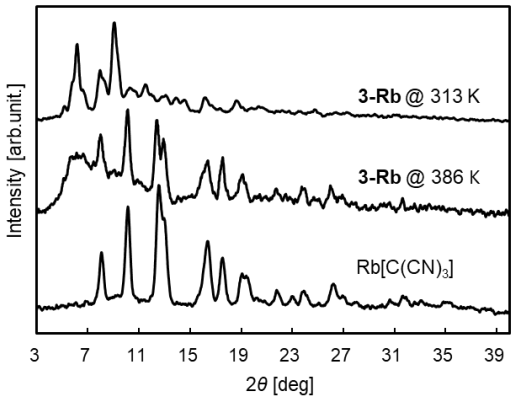

Fig. S6. Powder X-ray diffraction patterns of **3**–**Rb** (313 K, 386 K) and $Rb[C(CN)_3]$.

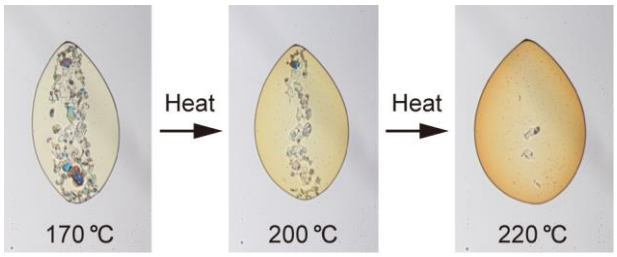

Fig. S7. Polarized micrographs of $[Ru(Cp)(C_6H_5C_2H_5)][Rb\{C(CN)_3\}_2]$ (**3**–**Rb**) taken upon heating after incongruent melting (T_m = 103 °C).

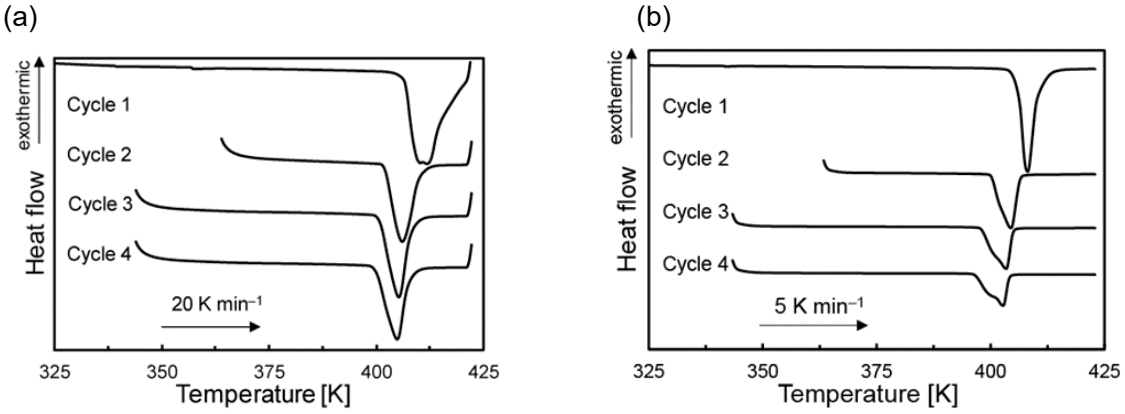

Fig. S8. DSC traces of incongruent melting process of $[Ru(Cp)(C_6H_5C_2H_5)][K\{C(CN)_3\}_2]$ (**3**–**K**) taken upon heating. (a) 20 K min^{-1}, (b) 5 K min^{-1}.

Table S1. Crystallographic parameters.

	1-K	**1-Rb**	**2-K**	**2-Rb**
Empirical formula	$C_{19}H_{11}N_6KRu$	$C_{19}H_{11}N_6RbRu$	$C_{20}H_{13}N_6KRu$	$C_{20}H_{13}N_6RbRu$
Formula weight	463.51	509.88	477.53	523.90
Crystal system	Monoclinic	Monoclinic	Triclinic	Triclinic
Space group	$P2_1/n$	$C2/m$	P-1	P-1
a [Å]	9.541(10)	12.9842(19)	8.3351(13)	8.3222(10)
b [Å]	17.385(18)	8.9304(13)	9.3330(15)	9.5142(12)
c [Å]	11.756(12)	9.5332(14)	13.271(2)	13.3112(17)
α [°]	90	90	100.751(2)	100.2990(10)
β [°]	105.900(15)	120.7640(10)	89.418(2)	91.2340(10)
γ [°]	90	90	91.514(2)	91.4330(10)
V [Å^3]	1875(3)	949.9(2)	1013.9(3)	1036.3(2)
Z	4	2	2	2
ρ_{calcd} [g cm^{-3}]	1.642	1.783	1.564	1.679
F(000)	920	496	476	512
Temperature [K]	100	100	100	100
Reflns collected	11032	2539	5325	5726
Independent reflns	4542	1032	3923	4263
Parameters	343	124	254	254
R(int)	0.0220	0.0270	0.0136	0.0104
R_1[a], R_w[b] ($I > 2\sigma$)	0.0359, 0.1074	0.0274, 0.0775	0.0185, 0.0488	0.0160, 0.0636
R_1[a], R_w[b] (all data)	0.0395, 0.1143	0.0275, 0.0777	0.0188, 0.0489	0.0164, 0.0648
Goodness of fit	1.061	1.086	1.092	0.605
$\Delta\rho_{max,min}$ [e Å^{-3}]	0.710, –1.647	0.682, –1.157	0.361, –0.518	0.374, –0.291

[a] $R_1 = \Sigma||F_o| - |F_c|| / \Sigma|F_o|$. [b] $R_w = [\Sigma w (F_o^2 - F_c^2)^2 / \Sigma w (F_o^2)^2]^{1/2}$.

Table S2. Crystallographic parameters.

	3-K	**4-K**	**5-K**	**6-Na**[c]
Empirical	$C_{21}H_{15}N_6KRu$	$C_{18}H_{10}N_6KCo$	$C_{18}H_{10}N_8B_2KCo$	$C_{14}H_{10}CoN_6Na$
Formula weight	491.56	408.35	457.99	344.20
Crystal system	Orthorhombic	Monoclinic	Monoclinic	Monoclinic
Space group	*Pbam*	*C*2/*m*	*C*2/*c*	*C*2/*c*
a [Å]	20.251(4)	12.885(4)	29.901(2)	23.954(11)
b [Å]	24.495(5)	8.563(2)	9.1624(7)	13.630(6)
c [Å]	8.4758(18)	9.184(3)	15.4190(12)	16.647(14)
α [°]	90	90	90	90
β [°]	90	120.273(2)	99.2340(10)	122.690(4)
γ [°]	90	90	90	90
V [Å^3]	4204.4(15)	875.1(4)	4169.5(6)	4574(5)
Z	8	2	8	12
ρ_{calcd} [g cm^{-3}]	1.553	1.550	1.459	1.499
F(000)	1968	412	1840	2088
Temperature [K]	100	100	100	100
Reflns collected	22433	1007	11509	11563
Independent	5133	997	4573	4909
Parameters	341	70	301	300
R(int)	0.0340	0.0345	0.0169	0.0500
R_1[a], R_w[b] ($I > 2\sigma$)	0.0426, 0.0941	0.0364, 0.0364	0.0233, 0.0622	0.1425, 0.4008
R_1[a], R_w[b] (all data)	0.0455, 0.0954	0.1205, 0.1205	0.0256, 0.0635	0.1551, 0.4162
Goodness of fit	1.258	1.129	1.057	1.797
$\Delta\rho_{max,min}$ [e Å^{-3}]	0.912, –1.280	0.645, –0.895	0.478, –0.318	5.085, –1.439

[a]$R_1 = \Sigma||F_o| - |F_c|| / \Sigma|F_o|$. [b]$R_w = [\Sigma w (F_o^2 - F_c^2)^2 / \Sigma w (F_o^2)^2]^{1/2}$. [c]Refinements were unsatisfactory due to the low quality of the crystal..